AGU PUBLICATIONS

Geophysical Research Letters

RESEARCH LETTER
10.1002/2014GL062982

Key Points:
- Fault roughness, not material heterogeneity, dominates rupture process
- Introduce parameter that can be used to quantify near-fault scattering
- Scattering affects the duration and amplitude of high-frequency ground motions

Supporting Information:
- Text S1
- Text S2
- Figure S1
- Figure S2
- Figure S3a
- Figure S3b
- Figure S4a
- Figure S4b
- Figure S5a
- Figure S5b
- Figure S6a
- Figure S6b
- Figure S7a
- Figure S7b
- Figure S8a
- Figure S8b

Correspondence to:
S. A. Bydlon,
sbydlon@stanford.edu

Citation:
Bydlon, S. A., and E. M. Dunham (2015), Rupture dynamics and ground motions from earthquakes in 2-D heterogeneous media, *Geophys. Res. Lett.*, *42*, 1701–1709, doi:10.1002/2014GL062982.

Received 25 DEC 2014
Accepted 12 FEB 2015
Accepted article online 16 FEB 2015
Published online 21 MAR 2015

Rupture dynamics and ground motions from earthquakes in 2-D heterogeneous media

Samuel A. Bydlon[1] and Eric M. Dunham[1,2]

[1]Department of Geophysics, Stanford University, Stanford, California, USA, [2]Institute of Computational and Mathematical Engineering, Stanford University, Stanford, California, USA

Abstract We perform 2-D simulations of earthquakes on rough faults in media with random heterogeneities (with von Karman distribution) to study the effects of geometric and material heterogeneity on the rupture process and resulting high-frequency ground motions in the near-fault region (out to ~20 km). Variations in slip and rupture velocity can arise from material heterogeneity alone but are dominantly controlled by fault roughness. Scattering effects become appreciable beyond ~3 km from the fault. Near-fault scattering extends the duration of incoherent, high-frequency ground motions and, at least in our 2-D simulations, elevates root-mean-square accelerations (i.e., Arias intensity) with negligible reduction in peak velocities. We also demonstrate that near-fault scattering typically occurs in the power law tail of the power spectral density function, quantified by the Hurst exponent and another parameter combining standard deviation and correlation length.

1. Introduction

High-frequency (~1–30 Hz) ground motions are of considerable interest to earthquake engineers. At these frequencies, the wavefield has a random character [*Housner*, 1947, 1955; *Haskell*, 1966; *Hanks and McGuire*, 1981; *Boore*, 1983] attributed to complexity in the earthquake source process and scattering by material heterogeneities at scales down to ~100 m. One purpose of this study is to examine the relative importance of source complexity and scattering on near-fault ground motions.

Initial studies of source complexity introduced random variations in slip and slip velocity with magnitude-dependent correlation lengths and times to explain far-field ground motion spectra [*Haskell*, 1966; *Aki*, 1967]. *Andrews* [1980, 1981] extended this work in his fractal source models lacking characteristic length scale or timescale. However, these models did not explicitly account for the causal spreading of the rupture, stress relaxation, and rupture dynamics.

Complementary work by *Madariaga* [1977, 1983], *Achenbach and Harris* [1978], and others used linear elastic fracture mechanics to explore the generation of high-frequency radiation from acceleration and deceleration of the rupture front. Building on these ideas, *Day* [1982] used 3-D dynamic rupture simulations to quantify variations in slip, slip velocity, and rupture velocity caused by nonuniform prestress conditions on planar faults. Considerable work has since extended these studies on source complexity and rupture dynamics. Most recently, *Dunham et al.* [2011b], building on geologic observations of fault surface roughness, performed 2-D dynamic rupture simulations of earthquakes on self-similar fractal faults. They found that observed levels of roughness introduce variations in slip and rupture velocity in a manner consistent with realistic high-frequency ground motions. Subsequent 3-D simulations by *Shi and Day* [2013] validated near-fault ground motions from simulated ruptures on rough faults by comparison to ground motion prediction equations calibrated with currently available strong motion records.

These studies, however, neglected off-fault material heterogeneity, which might alter the rupture process and ground motions. Before turning our attention to the random heterogeneities that are the focus of this work, we point out that material heterogeneity takes several forms. Most faults are surrounded by low-velocity zones; wave reflections and trapped waves within the low-velocity fault zone can influence the rupture process, leading to complex slip histories, rupture arrest, and even the formation of multiple slip pulses [*Harris and Day*, 1997; *Huang and Ampuero*, 2011]. Furthermore, Earth's crust has strong variations in properties with depth, which alters the seismic wavefield. However, in our study we focus solely on random variations in material properties that are responsible for scattering of waves along the propagation path.

The most obvious signature of scattering is the seismic coda, the decaying tail of oscillatory motions following direct wave arrivals [*Aki*, 1969]. Models of scattering are built on a stochastic description of random material heterogeneities, often together with a Born series expansion to quantify the amplitude and directional dependence of scattered waves [e.g., *Aki and Chouet*, 1975; *Sato*, 1977; *Wu*, 1985; *Zeng*, 1991; *Ryzhik et al.*, 1996].

Scattering effects are often included in broadband seismogram methods using the hybrid technique, in which a deterministic simulation for low-frequency waves is combined with a stochastic model for high-frequency waves. The resulting waveforms are then spliced together into a broadband synthetic seismogram [e.g., *Saikai and Somerville*, 1977; *Mai and Beroza*, 2003; *Graves and Pitarka*, 2004; *Liu and Archuleta*, 2006; *Mai et al.*, 2010; *Atkinson and Assatourians*, 2015; *Crempien and Archuleta*, 2015; *Graves and Pitarka*, 2015; *Olsen and Takedatsu*, 2015].

Direct simulation of the full broadband wavefield is also possible. *Frankel and Clayton* [1986] performed 2-D simulations of seismic waves in elastic media having spatial random heterogeneities superimposed on a uniform background material model. They examined several statistical models of heterogeneity and found that media with von Karman autocorrelation functions best explained two features seen in seismic recordings: teleseismic traveltime anomalies and the high-frequency (>30 Hz) content of the seismic coda in microearthquake waveforms. More recently, wave propagation simulations in random media have been done in 3-D [*Pitarka and Ichinose*, 2009; *Hartzell et al.*, 2010; *Imperatori and Mai*, 2013].

Our present study complements these efforts by introducing random material heterogeneities into 2-D dynamic rupture simulations of earthquakes on fractally rough faults. Our specific objective is to quantify the effects of source complexity and scattering on the rupture process and near-fault seismic wavefield. Because our models are done in 2-D, we accurately capture waves up to 30 Hz. We expect many of our conclusions, particularly regarding the influence of material heterogeneity on the rupture process, to extend to the more realistic 3-D case.

2. Simulation Specifications

Our 2-D plane strain dynamic rupture simulations are similar to those in *Dunham et al.* [2011a, 2011b], *Fang and Dunham* [2013], and *Trugman and Dunham* [2014]. Ruptures propagate along a nonplanar fault obeying a strong velocity-weakening friction law encapsulated in a rate-and-state framework. The off-fault material responds elastically until stresses exceed a Drucker-Prager yield condition, after which viscoplastic deformation occurs. This prevents fault opening and limits stress concentrations near geometric irregularities. Material and frictional properties are identical to those in *Dunham et al.* [2011a, 2011b]. For this study, we extended the numerical method of *Kozdon et al.* [2013] to handle spatially variable material properties. The method simply uses the local material properties; unlike with staggered grid methods, no averaging is required.

As in *Dunham et al.* [2011b], the fault is a band-limited self-similar fractal profile characterized by amplitude-to-wavelength ratio $\alpha = 10^{-2}$, indicating that root-mean-square deviations from planarity are 2 orders of magnitude smaller than the total profile length. (See Figures S1 and S2 in the supporting information.) The minimum wavelength of roughness is 200 m. The initial background stress field is uniform, and the maximum principal stress is inclined at an angle of 50° to the overall strike of the fault. Background normal and shear stresses (resolved onto the average fault plane) are 126 MPa and 42 MPa, respectively, for nonplanar fault simulations (126 MPa and 35 MPa for planar faults). Ruptures are artificially initiated at a localized overstressed asperity at the origin. We perform simulations for a 90 km by 90 km computational domain with 9 m grid spacing. The boundaries of the computational domain are padded by a perfectly matched layer [*Duru et al.*, 2014] to prevent artificial reflections.

3. Random Elastic Properties

In our simulations we introduce random fluctuations in elastic properties (density and *P* and *S* wave speeds) to a uniform background model. The statistical properties of the random field are defined by an autocorrelation function and the associated power spectral density function (PSDF). Following previous work [e.g., *Frankel and Clayton*, 1986; *Hartzell et al.*, 2010; *Imperatori and Mai*, 2013], we use an isotropic von

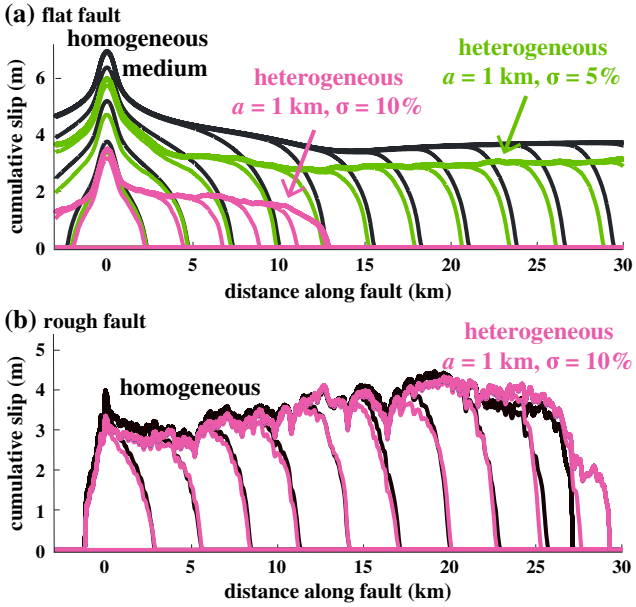

Figure 1. Cumulative slip (every 1 s) for ruptures on flat and rough faults in homogeneous and heterogeneous media. (a) Flat fault simulations demonstrate that material heterogeneity decreases slip and can cause rupture arrest near areas of high rigidity and density. (b) Rough fault simulations feature much larger fluctuations in slip and rupture velocity caused primarily by the complex fault geometry rather than material heterogeneity. Rupture arrests naturally in both directions by unfavorable bends in the fault; this happens immediately to the left of the hypocenter and after propagating about 30 km to the right.

Karman distribution for random properties. The 2-D von Karman PSDF for some property is

$$P(k) = \frac{4\pi\sigma^2 a^2 \nu}{(1 + k^2 a^2)^{\nu+1}}. \quad (1)$$

where k is the (radial) wave number, a is the correlation length, ν is the Hurst exponent, and σ is the standard deviation of the fluctuations, normalized by the mean value of that property. Thus, $P(k)$ represents the normalized PSDF of material property fluctuations, and we will explore wave speed fluctuations of $\sigma \approx 0$–20% in this study. The Hurst exponent controls the slope of the power law decay of the PSDF at high wave numbers.

An average value of 6 km/s is used for P wave speed and 3.464 km/s for S wave speed. The P and S wave speed perturbations are varied in an identical manner, with the same normalized standard deviation σ, such that Poisson's ratio remains constant (and equal to 0.25). The density is computed according to the regression equation relating P wave speeds (V_p, in km/s) and density (ρ, in g/cm^3) in [*Brocher*, 2005]

$$\rho(V_p) = 1.6612V_p - 0.4721V_p^2 + 0.0671V_p^3 - 0.0043V_p^4 + 0.000106V_p^5. \quad (2)$$

Several studies have been performed to constrain the parameters of the von Karman distribution (1). Sonic-log measurements in boreholes yield Hurst exponents $\nu \approx 0.1$–0.2 and correlation lengths on the order of tens to hundreds of meters [*Holliger*, 1996, 1997]. *Dolan and Bean* [1997] have noted, however, that small values for correlation length are controlled by the preprocessing or detrending of borehole data, making physical interpretation of the resultant values difficult. Studies based on interpretation of geologic maps yield $\nu \approx 0.2$–0.3 and correlation lengths ranging from meters to kilometers [*Holliger and Levander*, 1994; *Bean et al.*, 1999]. The preferred models of numerical simulation studies typically have correlation lengths of hundreds of meters to kilometers and Hurst exponents between 0 and 0.3 [*Frankel and Clayton*, 1986; *Nielsen and Thybo*, 2006; *Przybilla et al.*, 2009; *Imperatori and Mai*, 2013]. Throughout our study, we use a Hurst exponent of $\nu = 0.3$ but consider a range of different correlation lengths a and standard deviations σ.

4. Effects of Heterogeneity on Rupture Process

Our first objective is to assess the relative influence of off-fault material heterogeneity and fault roughness on variability in the rupture process. Results are summarized in Figure 1. Figure 1a shows cumulative slip on a flat fault embedded within either a homogeneous medium or one of two heterogeneous media (both with $a = 1$ km). The latter are characterized by $\sigma = 5\%$ and 10%. The background stress level, which is identical in all cases, is chosen around the minimum level required to obtain slip pulse ruptures. Heterogeneity of the material structure decreases average slip and rupture velocity and furthermore introduces small fluctuations in slip and rupture velocity. If the heterogeneity is strong enough and stress conditions are close to critical, ruptures can arrest, typically around areas of elevated rigidity and density.

We next introduce fault roughness, which requires increasing the background stress to obtain self-sustaining propagation [*Fang and Dunham*, 2013]. Figure 1b shows two simulations done on identical rough fault profiles, one in a homogeneous medium and the other in a heterogeneous medium. The

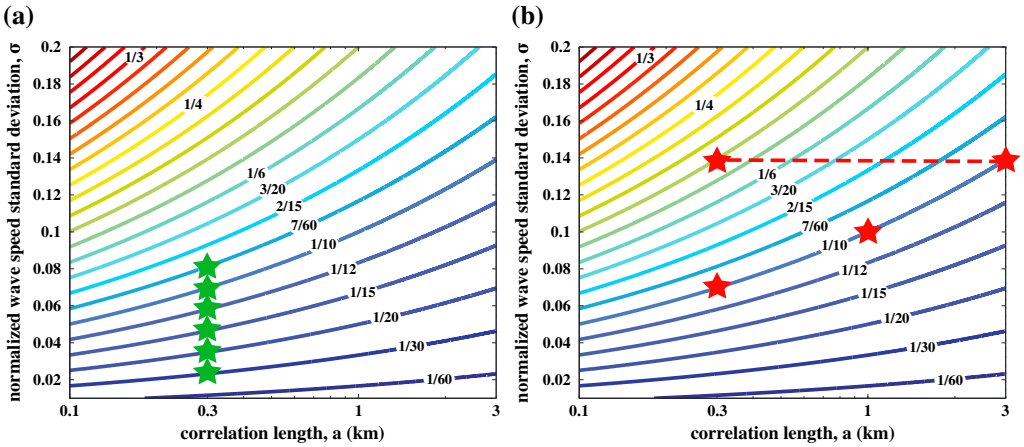

Figure 2. Contours of power law amplitude $p_0 = \sigma / a^{\nu}$ (units of km$^{-0.3}$) as a function of normalized wave speed standard deviation σ and correlation length a. (a) Experiment 1 determines minimum p_0 such that appreciable scattering effects are observed; a is held constant at 0.3 km, and p_0 is incremented in steps of 1/60 km$^{-0.3}$ between 1/30 and 7/60 km$^{-0.3}$ (green stars) by increasing σ. (b) Experiment 2 establishes that ground motions are nearly identical for constant p_0 = 1/10 km$^{-0.3}$, even if σ and a are different (red stars not connected by dotted line). Ground motions are also compared for identical σ but two different a and p_0 (red stars connected by dotted line).

heterogeneous medium is identical to that used in Figure 1a for the arresting rupture simulation ($a = 1$ km and $\sigma = 10\%$). Short-wavelength fluctuations in slip of comparable amplitude and phase appear in both cases and are much larger than those caused by material heterogeneity alone (Figure 1a). Examination of the fault profile itself establishes that these fluctuations are correlated with the fault slope, as discussed by *Dunham et al.* [2011b] and *Trugman and Dunham* [2014]. We therefore conclude that although material heterogeneity can influence the rupture process, complexity of the earthquake source process is dominated by the rough fault geometry.

5. Effects of Heterogeneity on Ground Motions

We next study the influence of scattering from material heterogeneities on ground motion in the near-fault region (out to about 20 km from the fault in our simulations). Our primary focus is on high-frequency (1–30 Hz) waves. Typical wavelengths of *S* waves in this frequency range are between 100 m and a few kilometers. Because scattering effects are most pronounced when seismic wavelengths are comparable to the length scale of material heterogeneities, we examine the power spectral density function (PSDF) at short wavelengths. For typical correlation lengths, the von Karman PSDF is well described in this limit by its power law tail. Taking the $ka \gg 1$ limit of the PDSF (1) yields

$$P(k) \approx \frac{4\pi\sigma^2\nu}{a^{2\nu}k^{2\nu+2}}. \tag{3}$$

The root-mean-square (RMS) fluctuation in normalized wave speed, for all wave numbers above some minimum wave number $k_{\min}$, is therefore given by

$$\sqrt{\frac{1}{2\pi}\int_{k_{\min}}^{\infty} P(k)k\mathrm{d}k} = \frac{\sigma}{(k_{\min}a)^{\nu}}. \tag{4}$$

In this limit, RMS fluctuations are inversely proportional to $k_{\min}^{\nu}$, with proportionality constant

$$p_0 = \sigma / a^{\nu}, \tag{5}$$

which we call the power law amplitude since it controls the amplitude of the power law tail of the von Karman PSDF. Figure 2 shows the parameter space of p_0 as a function of normalized standard deviation, σ, and correlation length, a. We hypothesize that p_0 controls the nature of scattering in the $ka \gg 1$ limit, regardless of the individual values of σ and a.

To test this hypothesis and to gain insight into the near-fault scattering process, we design a set of two numerical experiments. The first experiment (Figure 2a) establishes the minimum power law amplitude p_0

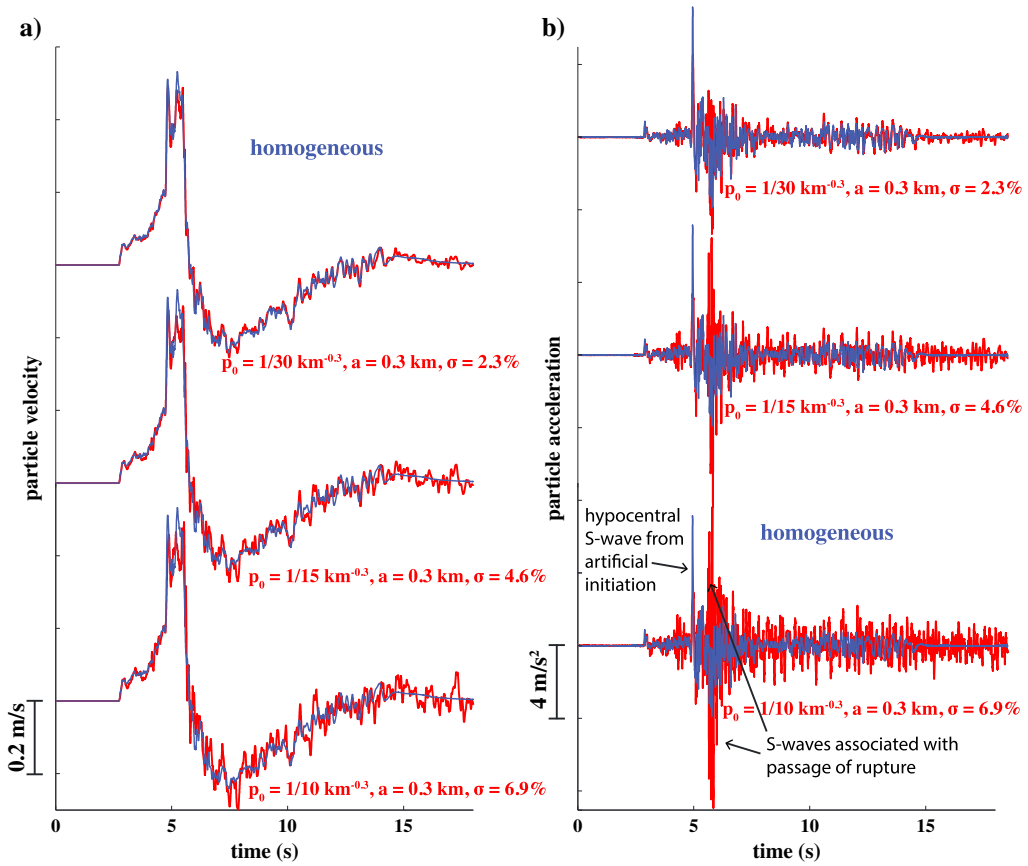

Figure 3. Seismograms from experiment 1 (Figure 2a): (a) fault-perpendicular velocities and (b) accelerations at a station located 15.3 km along strike from the hypocenter and 8.6 km off of the fault, comparing results in a homogeneous medium (blue) to those in heterogeneous media (red). Scattering causes negligible changes in peak velocities but increases peak and RMS accelerations, particularly for power law amplitudes $p_0 > 1/15$ km$^{-0.3}$. The acceleration spike from the artificial initiation process is unrealistic and should be ignored.

required to observe appreciable scattering effects. In the second experiment (Figure 2b) we first vary both σ and a while keeping p_0 constant; we expect seismograms to be nearly identical if our hypothesis is correct. To further confirm that the standard deviation, σ, is not the appropriate measure of heterogeneity amplitude, we compare two simulations with identical σ but different a (and hence different p_0). The seismograms are expected to be quite different.

We note here that p_0 is a dimensional quantity. In evaluating (5), we use the normalized σ and a in units of kilometers. Numerical values of p_0 are also specific to the chosen Hurst exponent $\nu = 0.3$ used throughout this study, although the overall concepts and conclusions are expected to generalize to other ν. We estimate $p_0 \approx 1/12$ km$^{-0.11}$ based on estimated von Karman parameter values reported in *Holliger* [1996] from the Cajon Pass borehole adjacent to the San Andreas Fault ($a = 0.14$ km, $\sigma = 6.65\%$, and $\nu = 0.11$).

In our first experiment, a series of rupture simulations are performed with identical rough fault profiles and background stresses in different random media. The correlation length is held fixed at $a = 0.3$ km as standard deviation σ is increased from 2.3% to 8.1%. This increases p_0 in increments of 1/60 km$^{-0.3}$ between 1/30 and 7/60 km$^{-0.3}$ (Figure 2a). The random media are generated using identical random number seeds, so the spatial pattern of heterogeneities is identical even though amplitudes are different. Ground motions (particle velocities and accelerations) are compared at a station located 8.6 km from the fault in the fault-perpendicular direction and 15.3 km from the hypocenter in the along-strike direction. This station location is sufficiently far from the fault that scattering effects are evident, and ground motions are representative of those at comparable distances. Results are shown in Figure 3. The overall

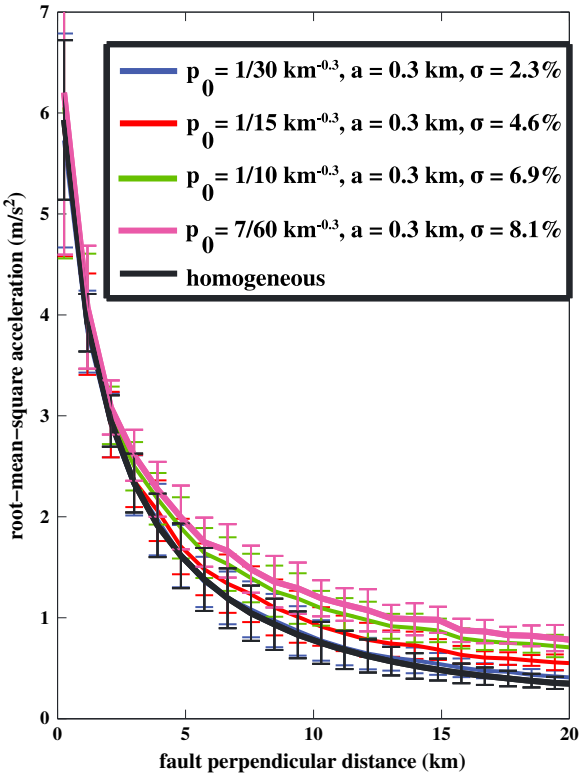

Figure 4. Spatially averaged RMS accelerations and standard deviations (error bars) as a function of fault-perpendicular distance for the heterogeneous media simulations in experiment 1 (Figure 2a). No differences are evident at distances less than 3 km. Beyond 3 km, RMS accelerations increase as p_0 increases. For $p_0 \geq 1/10$ km$^{-0.3}$, and distances greater than about 10 km, RMS accelerations in heterogeneous media consistently exceed those in a homogeneous medium (including one standard deviation bounds for both cases).

velocity waveform, which exhibits the well-known two-sided velocity pulse [e.g., *Aki*, 1968; *Dunham and Archuleta*, 2005], is only minimally altered by scattering. Peak velocities are nearly identical in homogeneous and heterogeneous media (see Figures S3–S8 in the supporting information). Scattering is most evident in the acceleration records, where it leads to elevated levels of sustained high-frequency shaking (i.e., the formation of the seismic coda). Note the acceleration spike associated with the *S* wave from the abrupt, artificial initiation process. This feature is not seen in actual ground motion records and should be ignored. Scattering increases sustained high-frequency accelerations by over a factor of 2 when the power law amplitude is increased to $p_0 = 1/10$ km$^{-0.3}$; in contrast, scattering is hardly evident for $p_0 = 1/30$ km$^{-0.3}$.

To quantify the increased accelerations from scattering, we compute the RMS acceleration over the interval $[t_s, 2t_s]$ where t_s is the direct *S* wave arrival time, as a function of fault-perpendicular distance. (We note that RMS accelerations are commonly used in the earthquake engineering literature in the closely related form of the Arias intensity [*Arias*, 1970].) The RMS acceleration values are spatially averaged in the fault-parallel direction at fixed fault-perpendicular distance. Specifically, we move away from the fault at intervals of 0.9 km (every 1000 grid points), and at each distance we compute the RMS acceleration for 34 points in the along-strike direction, spaced every 0.9 km (thus spanning about 30 km), starting around the hypocenter and ending close to where the rupture arrests. This excludes the region immediately ahead of the rupture, where directivity effects further amplify ground motions. The mean and standard deviation of these values are calculated and shown in Figures 4, 5c, and 5f.

The RMS accelerations from experiment 1 (Figure 2a) are shown in Figure 4. For distances less than 3 km, all simulations exhibit similar RMS acceleration values, suggesting that scattering is negligible this close to the fault over the modeled frequency range. For distances greater than 3 km, RMS accelerations begin to differ as p_0 is increased. The differences between the homogeneous and heterogeneous simulations become prominent around $p_0 = 1/15$ km$^{-0.3}$; when $p_0 \geq 1/10$ km$^{-0.3}$ and at distances greater than about 10 km, one standard deviation bounds for the simulations no longer overlap. We therefore conclude that near-fault scattering effects are significant at and above $p_0 = 1/10$ km$^{-0.3}$.

Having established a threshold p_0 for significant scattering in experiment 1, we now proceed in experiment 2 to verify that ground motions are nearly identical for heterogeneous media having identical p_0 but different a and σ. The set of three media with $p_0 = 1/10$ km$^{-0.3}$ used in this experiment are marked as red stars in Figure 2b, and results are summarized in Figures 5a–5c. There is a high degree of similarity between the velocity and acceleration seismograms for these three simulations, despite having an order of magnitude difference in correlation length, a, and a factor of 2 difference in standard deviation, σ, between the two most dissimilar media. The similarity is further seen when plotting spatially averaged RMS accelerations as a function of fault-perpendicular distance (Figure 5c).

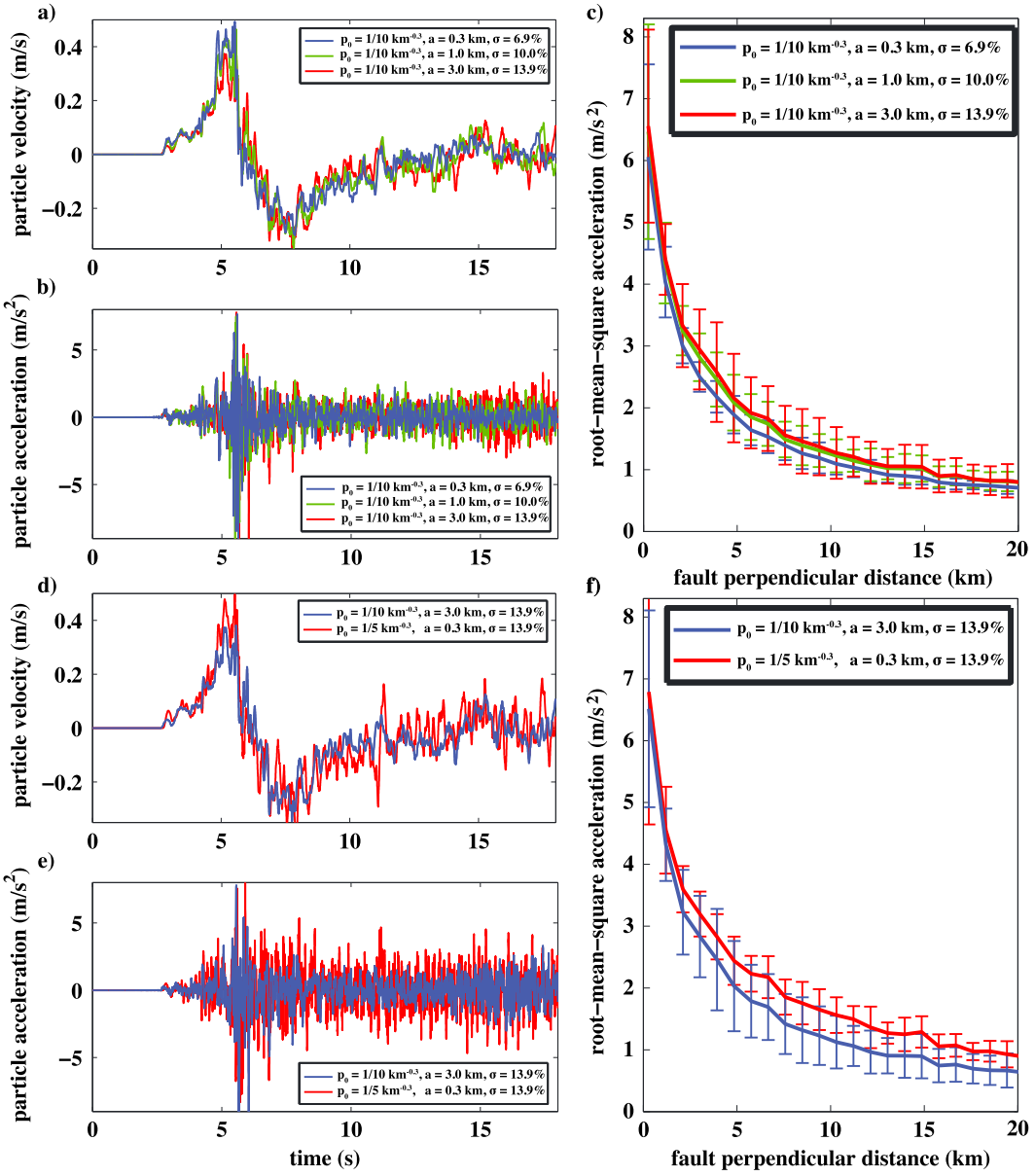

Figure 5. Results for experiment 2 (Figure 2b). In Figures 5a–5c, power law amplitude is held constant at $p_0 = 1/10$ km$^{-0.3}$ while σ and a are varied. Similarities of (a) velocity and (b) acceleration seismograms, as well as (c) RMS accelerations confirm that scattering is determined by p_0. In Figures 5d–5f, standard deviation is held constant at $\sigma = 13.9\%$ while a and p_0 are varied. Increased (d) velocities, (e) accelerations, and (f) RMS accelerations demonstrate that σ alone is insufficient to quantify scattering. Seismograms are at the same station used in Figure 3.

The final comparison, which serves as the second component of experiment 2, involves two media with identical values of σ but different a and therefore different p_0 (Figure 2b, red stars connected by dotted line). Seismograms and RMS accelerations are shown in Figures 5d–5f. Increasing p_0, even for identical σ, increases ground motion amplitudes associated with late-arriving scattered waves. To summarize, experiment 2 confirms that p_0 is the relevant amplitude parameter for quantifying high-frequency wave scattering in the near-fault region.

6. Conclusions

In this study we performed 2-D dynamic rupture simulations on rough faults in heterogeneous media. Material heterogeneities were generated using a von Karman distribution. We established that at the

short wavelengths (i.e., large wave numbers k) associated with scattering of high-frequency (1–30 Hz) seismic waves in the near-fault region, the von Karman distribution is well approximated as a power law. The amplitude of this power law is quantified in terms of the Hurst exponent, ν, and the power law amplitude, $p_0 = \sigma / a^{\nu}$, which combines the correlation length, a, and the standard deviation of fluctuations, σ. Numerical experiments confirm the utility of p_0 in characterizing near-fault scattering. But it is essential to note that p_0 is only effective in the $ka \gg 1$ limit; for smaller correlation lengths, both σ and a become independent parameters.

Our first important conclusion is that random heterogeneity of the off-fault material typically exerts little influence on the rupture process. Of course, for faults operating right around the minimum threshold stress for self-sustaining rupture, even small perturbations can lead to rupture arrest (Figure 1a). However, upon adding fault roughness to our simulations, we found that this geometric complexity led to substantially larger fluctuations in slip and rupture velocity than those caused by material heterogeneity. Provided that this result is also true in 3-D, then dynamic rupture simulations can safely neglect random material heterogeneities when solving for the rupture process.

In the next part of our study, we examined the effects of scattering on high-frequency ground motions. No effects are evident within approximately 3 km of the fault. And even beyond this distance, for representative values of heterogeneity, scattering causes negligible changes in peak ground velocity. In contrast, RMS accelerations are increased, sometimes by more than a factor of 2. This is potentially an important result but one that must be confirmed with similar 3-D simulations. Scattering effects are likely more pronounced in 3-D due to additional heterogeneities along components of the path in the third dimension. For example, even a station immediately adjacent to the fault will receive waves that have propagated ~10 km from the bottom edge of the fault.

Acknowledgments

This work was supported by the National Science Foundation (ACI-1148493), King Abdullah University of Science and Technology (KAUST) through a joint KAUST Academic Excellence Alliance (AEA) grant with Stanford, and the Southern California Earthquake Center. SCEC is funded by NSF Cooperative Agreement EAR-1033462 and USGS Cooperative Agreement G12AC20038. The SCEC contribution for this paper is 2064. We are grateful to Jeremy Kozdon for his assistance in extending the numerical method to heterogeneous media.

The Editor thanks Kim B. Olsen and an anonymous reviewer for their assistance in evaluating this paper.

References

Achenbach, J. D., and J. G. Harris (1978), Ray method for elastodynamic radiation from a slip zone of arbitrary shape, *J. Geophys. Res.*, *83*(B5), 2283–2291, doi:10.1029/JB083iB05p02283.

Arias, A. (1970), A measure of earthquake intensity, in *Seismic Design for Nuclear Power Plants*, edited by R. J. Hansen, pp. 438–483, MIT Press, Cambridge, Mass.

Atkinson, G. M., and K. Assatourians (2015), Implementation and validation of EXSIM (a stochastic finite-fault ground-motion simulation algorithm) on the SCEC broadband platform, *Seismol. Res. Lett.*, *86*(1), 48–60, doi:10.1785/0220140097.

Aki, K. (1967), Scaling law of seismic spectrum, *J. Geophys. Res.*, *72*(4), 1217–1231, doi:10.1029/JZ072i004p01217.

Aki, K. (1968), Seismic displacements near a fault, *J. Geophys. Res.*, *73*(16), 5359–5376, doi:10.1029/JB073i016p05359.

Aki, K. (1969), Analysis of the seismic coda of local earthquakes as scattered waves, *J. Geophys. Res.*, *74*(2), 615–631, doi:10.1029/JB074i002p00615.

Aki, K., and B. Chouet (1975), Origin of coda waves: Source, attenuation, and scattering effects, *J. Geophys. Res.*, *80*(23), 3322–3342, doi:10.1029/JB080i023p03322.

Andrews, D. J. (1980), A stochastic fault model: 1. Static case, *J. Geophys. Res.*, *85*(B7), 3867–3877, doi:10.1029/JB085iB07p03867.

Andrews, D. J. (1981), A stochastic fault model: 2. Time-dependent case, *J. Geophys. Res.*, *86*(B11), 10,821–10,834, doi:10.1029/JB086iB11p10821.

Bean, C. J., D. Marsan, and F. Martini (1999), Statistical measures of crustal heterogeneity from reflection seismic data: The role of seismic bandwidth, *Geophys. Res. Lett.*, *26*(21), 3241–3244, doi:10.1029/1999GL005400.

Boore, D. M. (1983), Stochastic simulation of high-frequency ground motions based on seismological models of the radiated spectra, *Bull. Seismol. Soc. Am.*, *73*(6A), 1865–1894.

Brocher, T. M. (2005), Empirical relations between elastic wavespeeds and density in the Earth's crust, *Bull. Seismol. Soc. Am.*, *95*(6), 2081–2092, doi:10.1785/0120050077.

Crempien, J. G. F., and R. Archuleta (2015), UCSB method for simulation of broadband ground motion from kinematic earthquake sources, *Seismol. Res. Lett.*, *86*(1), 61–67, doi:10.1785/0220140103.

Day, S. M. (1982), Three-dimensional simulation of spontaneous rupture: The effect of nonuniform prestress, *Bull. Seismol. Soc. Am.*, *72*(6a), 1881–1902.

Dolan, S. S., and C. J. Bean (1997), Some remarks on the estimation of fractal scaling parameters from borehole wire-line logs, *Geophys. Res. Lett.*, *24*(10), 1271–1274, doi:10.1029/97GL00987.

Dunham, E. M., and R. J. Archuleta (2005), Near-source ground motion from steady state dynamic rupture pulses, *Geophys. Res. Lett.*, *32*, L03302, doi:10.1029/2004GL021793.

Dunham, E. M., D. Belanger, L. Cong, and J. E. Kozdon (2011a), Earthquake ruptures with strongly rate-weakening friction and off-fault plasticity. Part 1: Planar faults, *Bull. Seismol. Soc. Am.*, *101*(5), 2296–2307, doi:10.1785/0120100075.

Dunham, E. M., D. Belanger, L. Cong, and J. E. Kozdon (2011b), Earthquake ruptures with strongly rate-weakening friction and off-fault plasticity. Part 2: Nonplanar faults, *Bull. Seismol. Soc. Am.*, *101*(5), 2308–2322, doi:10.1785/0120100076.

Duru, K., J. E. Kozdon, and G. Kreiss (2014), *Boundary Waves and Stability of the Perfectly Matched Layer. II: Extensions to First Order Systems and Numerical Stability*, Institutional Archive of the Naval Postgraduate School, Monterey, Calif.

Fang, Z., and E. Dunham (2013), Additional shear resistance from fault roughness and stress levels on geometrically complex faults, *J. Geophys. Res. Solid Earth*, *118*(7), 3642–3654, doi:10.1002/jgrb.50262.

Frankel, A., and R. W. Clayton (1986), Finite difference simulations of seismic scattering: Implications for the propagation of short-period seismic waves in the crust and models of crustal heterogeneity, *J. Geophys. Res.*, *91*(B6), 6465–6489, doi:10.1029/JB091iB06p06465.

Graves, R., and A. Pitarka (2004), Broadband time history simulation using a hybrid approach, paper presented at the 13th World Conference on Earthquake Engineering, Vancouver, Canada.
Graves, R. W., and A. Pitarka (2015), Refinements to the Graves and Pitarka (2010) broadband ground-motion simulation method, *Seismol. Res. Lett.*, *86*(1), 75–80, doi:10.1785/0220140101.
Hanks, T. C., and R. K. McGuire (1981), The character of high-frequency strong ground motion, *Bull. Seismol. Soc. Am.*, *71*(6), 2071–2095.
Harris, R. A., and S. M. Day (1997), Effects of a low-velocity zone on a dynamic rupture, *Bull. Seismol. Soc. Am.*, *87*(5), 1267–1280.
Hartzell, S., S. Harmsen, and A. Frankel (2010), Effects of 3D random correlated velocity perturbations on predicted ground motions, *Bull. Seismol. Soc. Am.*, *100*(4), 1415–1426, doi:10.1785/0120090060.
Haskell, N. (1966), Total energy and energy spectral density of elastic wave radiation from propagating faults. Part II: A statistical source model, *Bull. Seismol. Soc. Am.*, *56*(1), 125–140.
Holliger, K. (1996), Upper-crustal seismic velocity heterogeneity as derived from a variety of P-wave sonic logs, *Geophys. J. Int.*, *125*(3), 813–829, doi:10.1111/j.1365-246X.1996.tb06025.x.
Holliger, K. (1997), Seismic scattering in the upper crystalline crust based on evidence from sonic logs, *Geophys. J. Int.*, *128*(1), 65–72, doi:10.1111/j.1365-246X.1997.tb04071.x.
Holliger, K., and A. Levander (1994), Seismic structure of gneissic/granitic upper crust: Geological and petrophysical evidence from the Strona-Ceneri Zone (northern Italy) and implications for crustal seismic exploration, *Geophys. J. Int.*, *119*(2), 497–510, doi:10.1111/j.1365-246X.1994.tb00137.x.
Housner, G. W. (1947), Characteristics of strong-motion earthquakes, *Bull. Seismol. Soc. Am.*, *37*(1), 19–31.
Housner, G. W. (1955), Properties of strong ground motion earthquakes, *Bull. Seismol. Soc. Am.*, *45*(3), 197–218.
Huang, Y., and J.-P. Ampuero (2011), Pulse-like ruptures induced by low-velocity fault zones, *J. Geophys. Res.*, *116*, B12307, doi:10.1029/2011JB008684.
Imperatori, W., and P. Mai (2013), Broad-band near-field ground motion simulations in 3-dimensional scattering media, *Geophys. J. Int.*, *192*(2), 725–744, doi:10.1093/gji/ggs041.
Kozdon, J. E., E. M. Dunham, and J. Nordström (2013), Simulation of dynamic earthquake ruptures in complex geometries using high-order finite difference methods, *J. Sci. Comput.*, *55*, 92–124, doi:10.1007/s10915-012-9624-5.
Liu, P., and R. J. Archuleta (2006), Efficient modeling of Q for 3D numerical simulation of wave propagation, *Bull. Seismol. Soc. Am.*, *96*(4A), 1352–1358, doi:10.1785/0120050173.
Mai, M., and G. Beroza (2003), A hybrid method for calculating near-source, broadband seismograms: Application to strong motion prediction, *Phys. Earth Planet. Inter.*, *137*(1-4), 183–199, doi:10.1016/S0031-9201(03)00014-1.
Madariaga, R. (1977), High-frequency radiation from crack (stress drop) models of earthquake faulting, *Geophys. J. Int.*, *51*(3), 625–651, doi:10.1111/j.1365-246X.1977.tb04211.x.
Madariaga, R. (1983), High frequency radiation from dynamic earthquake fault models, *Ann. Geophys*, *1*(1), 17–23.
Mai, P. M., W. Imperatori, and K. B. Olsen (2010), Hybrid broadband ground-motion simulations: Combining long-period deterministic synthetics with high-frequency multiple S-to-S Backscattering, *Bull. Seismol. Soc. Am.*, *100*(5A), 2124–2142, doi:10.1785/0120080194.
Nielsen, L., and H. Thybo (2006), Identification of crustal and upper mantle heterogeneity by modelling of controlled-source seismic data, *Tectonophysics*, *416*(1), 209–228, doi:10.1016/j.tecto.2005.11.020.
Olsen, K., and R. Takedatsu (2015), The SDSU broadband ground-motion generation module BBtoolbox version 1.5, *Seismol. Res. Lett.*, *86*(1), 81–88, doi:10.1785/0220140102.
Pitarka, A., and G. Ichinose (2009), Simulating forward and backward scattering in viscoelastic 3D media with random velocity variations and basin structure, *Tech. Rep.*, U.S. Geol. Surv. Pasadena Calif.
Przybilla, J., U. Wegler, and M. Korn (2009), Estimation of crustal scattering parameters with elastic radiative transfer theory, *Geophys. J. Int.*, *178*(2), 1105–1111, doi:10.1111/j.1365-246X.2009.04204.x.
Ryzhik, L., G. Papanicolaou, and J. Keller (1996), Transport equations for elastic and other waves in random media, *Wave Motion*, *24*(4), 327–370, doi:10.1016/S0165-2125(96)00021-2.
Saikai, C. K., and P. G. Somerville (1977), Simulated hard-rock motions in Saint Louis, Missouri, from large New Madrid earthquakes (Mw 6.5), *Bull. Seismol. Soc. Am.*, *87*(1), 123–139.
Sato, H. (1977), Energy propagation including scattering effects single isotropic scattering approximation, *J. Phys. Earth*, *25*(1), 27–41.
Shi, Z., and S. Day (2013), Rupture dynamics and ground motion from 3-D rough-fault simulations, *J. Geophys. Res. Solid Earth*, *118*, 1122–1141, doi:10.1002/jgrb.50094.
Trugman, D., and E. Dunham (2014), A 2D pseudodynamic rupture model generator for earthquakes on geometrically complex faults, *Bull. Seismol. Soc. Am.*, *104*(1), 95–112, doi:10.1785/0120130138.
Wu, R. S. (1985), Multiple scattering and energy transfer of seismic waves—Separation of scattering effect from intrinsic attenuation: I. Theoretical modeling, *Geophys. J. Int.*, *82*(1), 57–80, doi:10.1111/j.1365-246X.1985.tb05128.x.
Zeng, Y. (1991), Compact solutions for multiple scattered wave energy in time domain, *Bull. Seismol. Soc. Am.*, *81*(3), 1022–1029.